



# Evaluation of Calibration Strategies for Accurate $\delta^{13}CH_4$ Measurements in Dry and Humid Air

Ji Li<sup>1,2,3</sup>, Xuguang Chi<sup>1,2</sup>, Aijun Ding<sup>1,2,3</sup>, Weimin Ju<sup>4</sup>, Yongguang Zhang<sup>4,5</sup>, Jing M. Chen<sup>6,7</sup>, Huilin Chen<sup>1,2,3</sup>\*

- 5 ¹Joint International Research Laboratory of Atmospheric and Earth System Sciences, School of Atmospheric Sciences, Nanjing University, Nanjing, China,
  - <sup>2</sup>Jiangsu Provincal Collorative Innovation Center of Climate Change, Nanjing, China
  - <sup>3</sup>Frontiers Science Center for Critical Earth Material Cycling, Nanjing University, Nanjing, 210023, China
- 4Jiangsu Provincial Key Laboratory of Geographic Information Science and Technology, Key Laboratory for Land Satellite Remote Sensing Applications of Ministry of Natural Resources, School of Geography and Ocean Science, Nanjing University, Nanjing, Jiangsu, China
  - <sup>5</sup>Jiangsu Center for Collaborative Innovation in Geographical Information Resource Development and Application, International Institute for Earth System Sciences, Nanjing University, Nanjing, Jiangsu 210023, China
  - <sup>6</sup>School of Geographical Science, Key Laboratory for Humid Subtropical Eco-Geographical Processes of the Ministry of Education, Fujian Normal University, Fuzhou 350008, China
  - <sup>7</sup>Department of Geography and Planning, University of Toronto, Toronto, ON M5S 3G3, Canada

Corresponding to: Huilin Chen (huilin.chen@nju.edu.cn)

**Abstract.** Accurate determination of the methane isotopic composition ( $\delta^{13}$ CH<sub>4</sub>) is essential for 20 attributing emission sources of methane (CH<sub>4</sub>). However, for measurements with optical instruments, spectral interference from water vapor and instrumental drift often introduces substantial biases in  $\delta^{13}CH_4$ measurements, particularly for humid air measurements. Although multiple calibration strategies exist, a systematic evaluation of their performance under diverse field conditions remains lacking. Here, we evaluate two calibration strategies for a cavity ring-down spectrometer: a delta-based calibration for δ13CH<sub>4</sub> and an isotopologue-specific calibration for <sup>12</sup>CH<sub>4</sub> and <sup>13</sup>CH<sub>4</sub>. We performed laboratory experiments over a water vapor range of 0.15-4.0% to establish empirical correction functions, quadratic for <sup>12</sup>CH<sub>4</sub> and <sup>13</sup>CH<sub>4</sub>, and linear for δ<sup>13</sup>CH<sub>4</sub>, to remove humidity-induced biases. These correction functions were then applied to field measurements in both dried air at the SORPES stie and humid air at the Jurong site. At the SORPES site where air samples were dried using a Nafion<sup>TM</sup> dryer, the mean difference in  $\delta^{13}$ CH<sub>4</sub> between the two strategies was ~0.29 \( \text{\omega} \). In contrast, for humid air at the Jurong site, significant inter-method biases were observed, with  $\Delta\delta^{13}CH_4$  exhibiting a strong correlation with 1/CH<sub>4</sub>, indicating non-linear spectral effects at high concentrations that compromise the performance of delta-based calibration. Notably, only the isotopologue-specific calibration, coupled with an explicit water vapor correction, delivered stable and accurate  $\delta^{13}CH_4$  measurements across all conditions. This 35 work underscores the need for robust calibration strategies to minimize bias in CH4 isotopic composition

Key words: δ<sup>13</sup>CH<sub>4</sub>; calibration strategies; water vapor correction; cavity ring-down spectroscopy





#### 1. Introduction

60

65

70

75

Methane (CH<sub>4</sub>) is a potent greenhouse gas that plays a key role in climate change, contributing 40 approximately 16.4% of total anthropogenic radiative forcing (Patra and Khatri, 2022). Its global warming potential is about 28 times greater than that of carbon dioxide (CO<sub>2</sub>) over a 100-year time horizon, making CH<sub>4</sub> a critical target for near-term climate mitigation (Forster et al., 2021; Nisbet et al., 2020; Van Dingenen et al., 2018; Shindell et al., 2012; Ipcc, 2007). The primary sources of CH<sub>4</sub> emissions are direct anthropogenic activities (e.g., agriculture, waste, fossil fuels, and biomass burning), and natural and indirect anthropogenic sources, including wetlands, inland waters, and geological seepage. In 45 contrast, its removal from the atmosphere is mainly governed by oxidation with hydroxyl radicals (OH) (Kirschke et al., 2013; Olivier and Berdowski, 2021; Saunois et al., 2020). However, substantial uncertainties remain in these estimates: 20-35% for anthropogenic sources, ~50% for wetlands and biomass burning, up to 100% for inland waters and geological sources, and 10-20% for the OH sink 50 (Saunois et al., 2025). To constrain budgets and design effective reduction strategies, it is essential to distinguish between its diverse emission sources.

The carbon isotopic composition of CH<sub>4</sub> (δ<sup>13</sup>CH<sub>4</sub>) provides valuable constraints on tracking emission sources (Nisbet et al., 2016; Rice et al., 2016; Schaefer et al., 2016), as microbial, thermogenic, and pyrogenic origins exhibit distinct isotopic signatures (Levin et al., 1993; Bakkaloglu et al., 2022; Ehleringer and Osmond, 1989). δ<sup>13</sup>CH<sub>4</sub>-based analysis enables classification of emission types and supports quantitative estimation of CH<sub>4</sub> emissions on regional to global scales (De Groot, 2004; Saunois et al., 2020; Lan et al., 2021). However, these applications critically depend on high-precision isotopic measurements, since even small observational biases can propagate into large errors in inferred source signatures (Iaea., 2024; Defratyka et al., 2025; France et al., 2022).

Conventionally,  $\delta^{13}$ CH<sub>4</sub> has been measured using isotope ratio mass spectrometry (IRMS), which provides high precision measurements ( $\leq 0.1$  %) but requires labor-intensive sampling and lacks continuous coverage (Miller et al., 2002; Schaefer et al., 2006; Röckmann et al., 2016). Recent advances in laser-based spectroscopy, particularly cavity ring-down spectroscopy (CRDS) and quantum cascade laser absorption spectroscopy (QCLAS), have enabled in situ and automated  $\delta^{13}$ CH<sub>4</sub> monitoring (Rella et al., 2015; Tuzson et al., 2008). While these techniques offer advantages over conventional IRMS, their measurement accuracy is challenged by spectroscopic interferences, such as water vapor, and by the choice of calibration strategies. This is true whether  $\delta^{13}$ CH<sub>4</sub> is adjusted directly or is derived from isotopologue-specific calibrations, as highlighted in subsequent evaluations (Griffith, 2018; Hoheisel et al., 2019; Saboya et al., 2022).

Water vapor affects measured CH<sub>4</sub> mole fractions through dilution and spectral interference, thereby introducing systematic biases in isotopologue-based measurements (Chen et al., 2010; Hoheisel et al., 2019; Saboya et al., 2022). Consequently, whether the sampled air is dried prior to analysis critically affects the accuracy of  $\delta^{13}$ CH<sub>4</sub> measurements, a factor that becomes particularly important in humid environments. In addition, two primary calibration strategies have been developed to retrieve  $\delta^{13}$ CH<sub>4</sub> from laser-based spectroscopic observations (Wen et al., 2013; Griffith, 2018; Griffith et al., 2012; Flores et al., 2017; Tans et al., 2017). One is a direct correction of  $\delta^{13}$ CH<sub>4</sub> (hereafter, *delta-based correction*), which is relatively straightforward but may retain residual artifacts linked to CH<sub>4</sub> concentration (Wen et

85

90

95

110





al., 2013; Pang et al., 2016; Griffith et al., 2012; Braden-Behrens et al., 2017; Flores et al., 2017). Another one is isotopologue-specific correction for  $^{12}\text{CH}_4$  and  $^{13}\text{CH}_4$  (hereafter, *isotopologue-specific correction*), in which  $\delta^{13}\text{CH}_4$  is derived from independently corrected isotopologue concentrations, thereby reducing concentration-dependent biases (Griffith, 2018; Wen et al., 2013).

As water vapor remains a dominant limitation for accurate δ<sup>13</sup>CH<sub>4</sub> measurement, physical drying to approximately < 0.1%  $H_2O$  (dew point  $\approx$  -25 °C) is generally recommended to obtain high-precision  $\delta^{13}$ CH<sub>4</sub> measurements at the sub-per-mil level (Rella et al., 2015). Laboratory studies demonstrated a quadratic CH<sub>4</sub> - H<sub>2</sub>O relationship, indicating that water vapor affects CH<sub>4</sub> through both dilution and spectral interference (Chen et al., 2010; Rella et al., 2013), and a cross-sensitivity of ~0.54 ‰ per 1% H<sub>2</sub>O within 0.15-1.5% H<sub>2</sub>O (Hoheisel et al., 2019). In comparison, Saboya et al. (2022) applied a linear  $\delta^{13}CH_4$  correction over 0–2.2%  $H_2O$  and found  $CH_4$  mole fractions to be unaffected by water vapor within this range, while Chen et al. (2010) reported a clear quadratic dependence across 0.6-6% H<sub>2</sub>O. Moreover, explicit correction functions for the individual isotopologues (12CH<sub>4</sub> and 13CH<sub>4</sub>) remain lacking, and the δ<sup>13</sup>CH<sub>4</sub> corrections vary widely in form, highlighting the need for more robust approaches. Both calibration strategies ideally rely on multi-point calibration using reference gases that span the targeted range, either in mole fractions of  $^{12}\text{CH}_4$  and  $^{13}\text{CH}_4$  (for isotopologue-specific calibration) or in  $\delta^{13}\text{CH}_4$ (for delta-based calibration) (Wen et al., 2013; Griffith, 2018), but practical limitations persist. Deltabased correction is constrained by scarce isotopic standards (Griffith, 2018) and prone to concentrationdependent biases (Wen et al., 2013; Griffith, 2018), while isotopologue-specific correction can reduce such concentration dependence but lacks well-established water correction functions for <sup>12</sup>CH<sub>4</sub> and <sup>13</sup>CH<sub>4</sub>. These methodological gaps are particularly critical in humid environments, where water vapor effects are often large.

In this study, we aim to evaluate isotopologue-specific and delta-based calibration strategies for obtaining accurate  $\delta^{13}\text{CH}_4$  measurements in both dry and humid air. To achieve this, we conducted water vapor laboratory experiments to derive empirical correction functions for  $^{12}\text{CH}_4$ ,  $^{13}\text{CH}_4$ , and  $\delta^{13}\text{CH}_4$ . These corrections were then applied to field measurements to assess the accuracy of both calibration strategies for measurements in both dry and humid air.

## 105 2. Materials and Methods

## 2.1 The $\delta^{13}$ C-CH<sub>4</sub> analyzer

The  $\delta^{13}$ C-CH<sub>4</sub> analyzer used in this study was a G2201-i instrument manufactured by Picarro Inc. (Santa Clara, CA, USA). This instrument is based on the cavity ring-down spectroscopy (CRDS) technique, which enables real-time measurements of CH<sub>4</sub> and CO<sub>2</sub> isotopologues ( $^{12}$ CH<sub>4</sub>,  $^{13}$ CH<sub>4</sub>,  $^{12}$ CO<sub>2</sub>,  $^{13}$ CO<sub>2</sub>). CRDS quantifies gas absorption by measuring the exponential decay rate of light intensity in a high-reflectivity optical cavity, providing high sensitivity and strong resistance to external interference (Crosson, 2008; Berden and Engeln, 2009; Crosson et al., 2002; Wahl et al., 2006). Here, we evaluate observations of both CH<sub>4</sub> mole fractions and  $\delta^{13}$ C-CH<sub>4</sub> values derived from  $^{12}$ CH<sub>4</sub> and  $^{13}$ CH<sub>4</sub> measurements.

115 The instrument is equipped with a dual-laser module that allows automatic switching between CH<sub>4</sub> and

125

130

135

150





 $CO_2$  isotopologue measurements. During experiments covering a humidity range of 0-4.0%, the cavity temperature and pressure remained highly stable ( $45.000 \pm 0.001^{\circ}C$  and  $197.317 \pm 0.084$  hPa, respectively). The analyzer includes an internal water vapor correction algorithm that compensates for humidity effects for the calculation of  $\delta^{13}CH_4$ . According to the manufacturer's white paper, this correction is internally applied to the  $^{12}CH_4$  signal before computing  $\delta^{13}CH_4$ , using an empirically derived function to adjust for  $H_2O$ -induced spectral interference (Picarro, 2012; Rella, 2012). As a result,  $\delta^{13}CH_4$  values are indirectly adjusted for humidity, whereas the raw  $^{12}CH_4$  and  $^{13}CH_4$  mole fractions remain uncorrected and represent humid-air concentrations.

#### 2.2 Experimental design and measurement system

## 2.2.1 Water vapor correction

To quantify and correct for the influence of water vapor on the  $\delta^{13}\text{CH}_4$  measurements, we performed a water vapor laboratory experiment using a Picarro G2201-i analyzer (Fig. 1a), following a modified setup from Rella et al. (2013). A cotton filter soaked with deionized water was placed at the inlet to gradually humidify the sample stream, forming an artificially humidified phase to derive empirical water vapor correction functions for  $^{12}\text{CH}_4$ ,  $^{13}\text{CH}_4$ , and  $\delta^{13}\text{CH}_4$ . The analyzer continuously sampled a reference gas (Ref0, Table 1) at a flow rate of ~45 mL min<sup>-1</sup> for approximately six hours, during which water vapor mole fraction decreased from ~4.0% to ~0.1%. Over the entire experiment, the instrument drift between the two dry-reference periods was 1.8 ppb (0.092 %) for  $^{12}\text{CH}_4$ , 0.02 ppb (0.095 %) for  $^{13}\text{CH}_4$ , and 0.262 % for  $\delta^{13}\text{CH}_4$  (Fig. 2). Empirical relationships between measured signals and H<sub>2</sub>O concentration were then derived. For  $^2\text{CH}_4$  and  $^{13}\text{CH}_4$ , second-order polynomial fits were applied (Chen et al., 2010; Rella et al., 2013), while  $\delta^{13}\text{CH}_4$  was corrected using a linear regression (Hoheisel et al., 2019). These correction functions were subsequently applied to both reference and field measurements to remove H<sub>2</sub>O-induced spectral interference.

## 2.2.2 Field observations

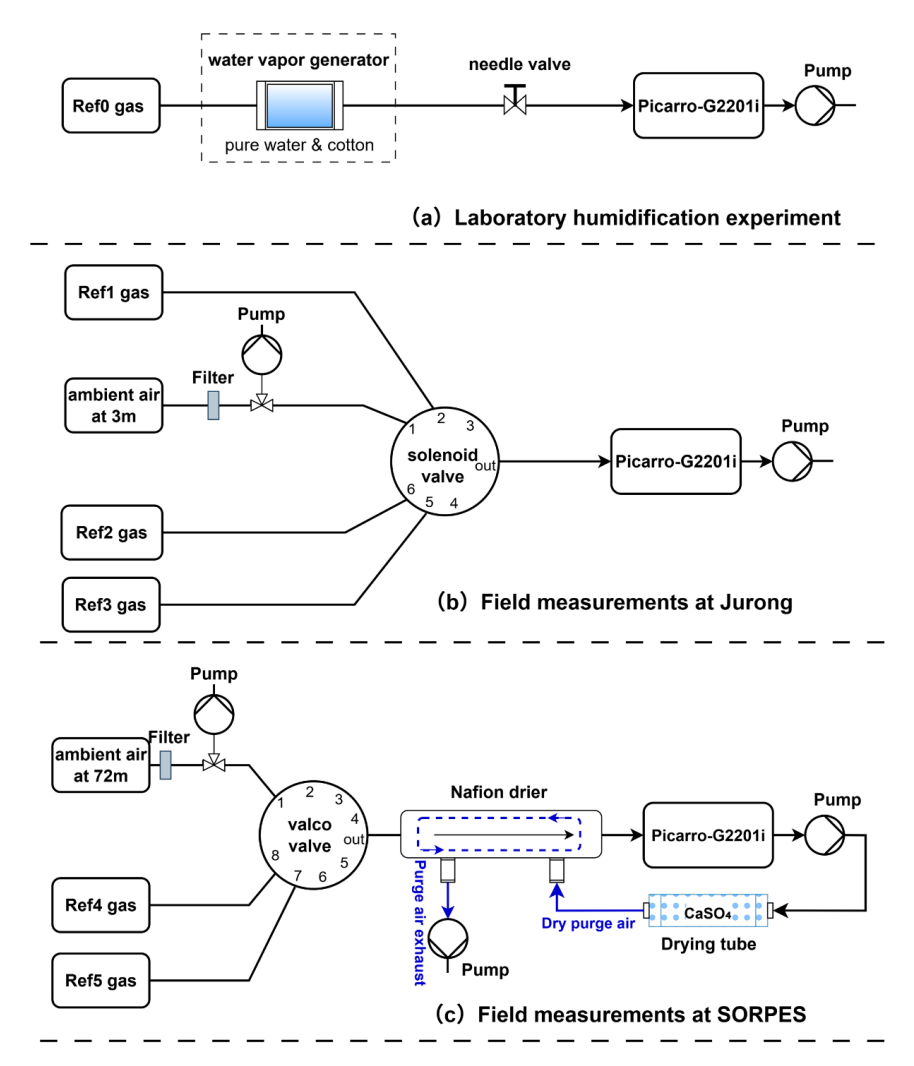
The δ¹³CH₄ measurement system was deployed at two sites in the Yangtze River Delta (Fig. 1b, c; Table 2). The Station for Observing Regional Processes of the Earth System (SORPES) station, located on the Xianlin campus of Nanjing University (118°57′10″E, 32°07′14″N; ~40 m a.s.l.), represents a regional background site influenced by large-scale anthropogenic emissions (Ding et al., 2016). The Jurong station (31°48′24.59″N, 119°13′2.15″E) is situated in an irrigated rice paddy and characterizes an agricultural ecosystem under a subtropical monsoon climate (Li et al., 2020).

At both sites, ambient CH<sub>4</sub> and δ<sup>13</sup>CH<sub>4</sub> were recorded at 0.5 Hz and aggregated to 5-min means. Reference gases were introduced every six hours to ensure accuracy while conserving calibration gases. Humidity conditions contrasted strongly between two sites: SORPES used a Nafion<sup>TM</sup> membrane dryers (Perma Pure, USA) to maintain stable H<sub>2</sub>O (0.04–0.40%), whereas Jurong operated without drying, resulting in elevated H<sub>2</sub>O (0.93–3.5%) consistent with the paddy environment. Calibration approaches also differed. At Jurong, ambient measurements were corrected using linear interpolation between Ref1 and Ref3 to cover a wide CH<sub>4</sub> and δ<sup>13</sup>CH<sub>4</sub> span. At SORPES, where Ref4 and Ref5 were similar in





composition, a single-point correction based on Ref8 was applied.



155 **Fig. 1 Laboratory and field setups for CH<sub>4</sub> and δ¹³CH<sub>4</sub> measurements using a Picarro G2201-i analyzer.** (a) Laboratory setup for deriving the water vapor correction function using humidified Ref0 gas (same composition as Ref7). (b) Field setup at the Jurong site using Ref1–Ref3 and ambient air at 3m above the ground, switched via a solenoid valve. (c) Field setup at the SORPES site with Ref5–Ref6 and ambient air sampled at 72 m above the ground, equipped with a Nafion<sup>TM</sup> dryer.

# 160 2.2.3 Reference gas measurements

Reference gases were measured in the laboratory and at both field sites to evaluate the performance of the calibration strategies and to ensure consistency of ambient air measurements (Fig. 1b–d). In the laboratory, three reference gases (Ref6–Ref8) were analyzed for 30 min each, while at the Jurong and SORPES sites, three (Ref1–Ref3) and two (Ref4–Ref5) reference gases were measured, respectively.

175





Each field measurement lasted 10 min, and the final 5 min were averaged for analysis. At Jurong, where no drying was applied, reference gases became humidified in the sampling lines; these values were first corrected for H<sub>2</sub>O interference before calibration. A detailed description of all reference gases is given in Table 1.

To assess calibration performance, mid-level references (Ref2 at Jurong and Ref7 in the laboratory) were treated as "targets," while the remaining references were used for calibration. Correction coefficients derived from linear interpolation between reference and measured values were then applied to the target periods.

All reference gas values used in this study, across both laboratory and field experiments, were traceable to internationally recognized calibration scales. CH<sub>4</sub> mole fractions were reported on the World Meteorological Organization (WMO) X2004A scale, and  $\delta^{13}$ CH<sub>4</sub> values were reported relative to the Vienna Pee Dee Belemnite (VPDB) scale, calibrated against working standards linked to the Institute of Arctic and Alpine Research (INSTAAR, University of Colorado Boulder) laboratory scale. The calibration and correction methods applied to these datasets are described in Section 2.3.

Table 1 Certified values of CH4 molar fraction and  $\delta 13 \text{CH4}$  for dry and humidified reference gases.

Reference Standard	CH <sub>4</sub> (ppb)	δ <sup>13</sup> CH <sub>4</sub> (‰)	<sup>13</sup> r	$\mathbf{R}_{ ext{sum}}$	<sup>12</sup> CH <sub>4</sub> (ppb) True v	13CH <sub>4</sub> (ppb) ralues
Ref0	1979.9	-48.14	0.01064203	1.011208816	1957.95	20.84
Ref1	2004.32	-46.80	0.010656929	1.011223724	1982.07	21.12
Ref2	3592.80	-47.01	0.010654656	1.011221449	3552.93	37.86
Ref3	5017.03	-47.16	0.010652979	1.011219770	4961.36	52.85
Ref4	1985.35	-48.00	0.010645125	1.011274904	1963.34	20.90
Ref5	1983.94	-49.06	0.010632171	1.011261942	1961.97	20.86
Ref6	1831.6	-47.85	0.010645205	1.011211993	1811.29	19.28
Ref7	1979.9	-48.14	0.01064203	1.011208816	1957.95	20.84
Ref8	2219.2	-45.98	0.01066609	1.011232889	2194.55	23.41

Note: CH<sub>4</sub> and  $\delta^{13}$ CH<sub>4</sub> are certified values for each standard gas. 13r denotes the ratio between <sup>13</sup>CH<sub>4</sub> and <sup>12</sup>CH<sub>4</sub>, calculated from Eq. (5). R<sub>sum</sub> is the total isotopologue normalising factor for methane, defined in Eq (6). This correction accounts for the absorption effects introduced by the presence of hydrogen isotopologues such as CH3D in atmospheric methane, in addition to carbon isotopologues.

Table 2. Summary of observation settings at the SORPES and Jurong stations.

Site	Environmental Conditions	Target Sample	Selected Period
SORPES	Urban background, low humidity $(H_2O:\ 0.04\%-0.40\%)$	From the environment air at 70.0 m	DOY240 ~ 280 in 2022
Jurong	Rice paddy, high humidity $(H_2O: 0.93\% - 3.5\%)$	From rice canopy at 3.0 m	DOY 240 ~ 280 in 2018

185



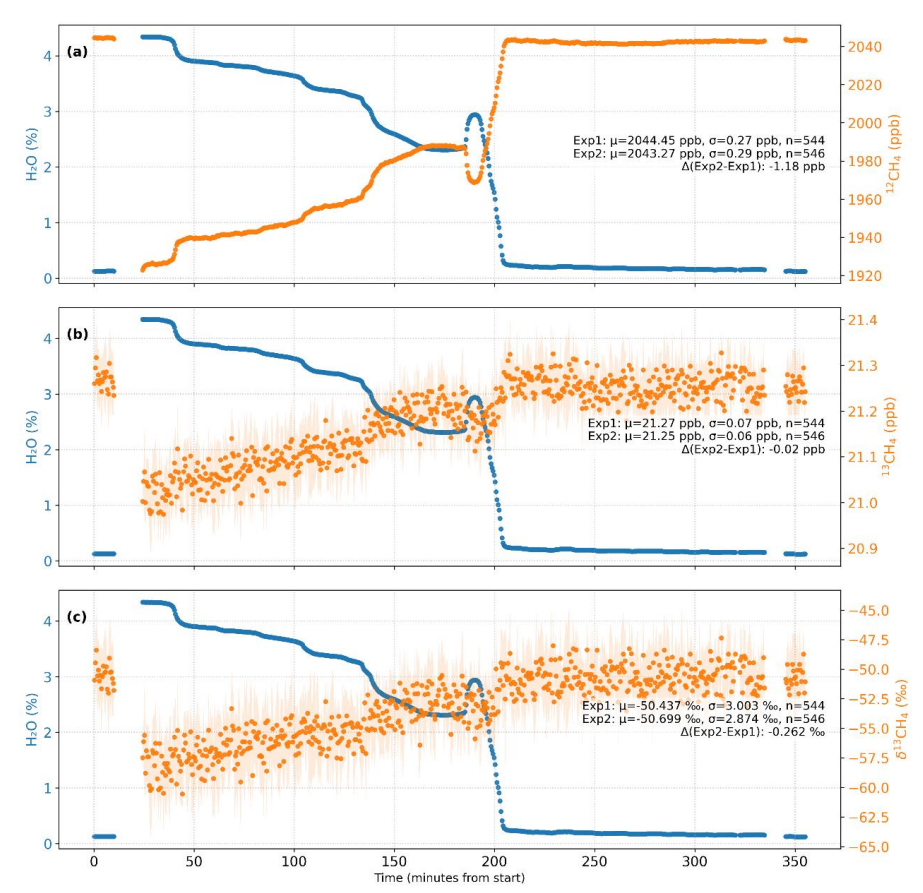


Fig. 2 Time series of  $H_2O$ ,  $^{12}CH_4$ ,  $^{13}CH_4$ , and  $\delta^{13}CH_4$  during the controlled humidity experiment. Each point represents a 30 s mean value, and the shaded areas indicate the  $1\sigma$  standard deviation of each bin. Exp1 and Exp2 correspond to the dry reference gas measurements performed before and after the artificially humidified period, respectively. The annotated statistics in each panel show the mean  $(\mu)$ , standard deviation  $(\sigma)$ , number of averaged points (n), and the drift  $(\Delta Exp2-Exp1)$ , demonstrating the measurement stability of  $^{12}CH_4$ ,  $^{13}CH_4$ , and  $\delta^{13}CH_4$  across the humidified period.  $H_2O$  represents the water vapor mole fraction (in %).

## 2.3 Calibration and correction strategies

190

195

Following the water vapor correction, two calibration strategies were applied to derive  $\delta^{13}CH_4$  from the analyzer outputs, which were the isotopologue-specific calibration approach (Wen et al., 2013; Griffith, 2018) and the direct  $\delta^{13}CH_4$  calibration method (delta-based). These methods were evaluated under both dry and humidified reference gas conditions.

# 2.3.1 Isotopologue-specific calibration

This method involves two steps:

200 (1) Separate linear correction equations were established for <sup>12</sup>CH<sub>4</sub> and <sup>13</sup>CH<sub>4</sub> using two reference gases with significantly different isotopologue concentrations. Calibration coefficients a and b were determined from the linear relationship between calibrated and observed values. (2) These coefficients were





subsequently applied to the target sample measurements to calculate the total  $CH_4$  concentration and  $\delta^{13}CH_4$  values using the following equations:

$$^{12}CH_{4,ture} = a_{12} \times ^{12}CH_{4,dry} + b_{12} \tag{1}$$

$$^{13}CH_{4,ture} = a_{13} \times ^{13}CH_{4,dry} + b_{13} \tag{2}$$

$$\delta^{13}CH_{4,cal} = \left(\frac{^{13}r}{^{13}r_{ref}} - 1\right) \times 1000\%$$
 (3)

$$CH_4 = {}^{12}CH_4 \times R_{sum} \tag{4}$$

$$^{13}r = ^{13}CH_4/^{12}CH_4 \tag{5}$$

$$R_{sum} = (1 + {}^{13}r)(1 + {}^{2}r)^{4} \tag{6}$$

$${}^{2}r = {}^{2}r_{ref} \times \left(\frac{\delta_{\rm D}}{1000} + 1\right) = 0.00014018 \tag{7}$$

To perform the correction, the mole fractions of <sup>12</sup>CH<sub>4</sub> and <sup>13</sup>CH<sub>4</sub>, as well as the δ<sup>13</sup>CH<sub>4</sub>, and δD-CH<sub>4</sub> values of each reference gas, must be known. Here, <sup>12</sup>CH<sub>4</sub> and <sup>13</sup>CH<sub>4</sub> represent the measured mole fractions (ppb) of the two carbon isotopologues of CH<sub>4</sub>, obtained directly from the spectrometer under dry air conditions. CH<sub>4</sub> in Eq. (4) denotes the total methane mole fraction, i.e., the sum of all isotopologues. δ<sup>13</sup>CH<sub>4</sub> (‰, VPDB scale) and δD–CH<sub>4</sub> (‰, Vienna Standard Mean Ocean Water, VSMOW scale) denote the carbon and hydrogen isotopic compositions of methane, respectively, determined based on certified reference gases or previous intercomparison results. Constants used in the calculations included <sup>13</sup>r<sub>ref</sub>=0.0111802 (VPDB) and <sup>2</sup>r<sub>ref</sub>=0.00015575 (VSMOW), which are the internationally accepted reference isotope ratios for <sup>13</sup>C/<sup>12</sup>C and D/H, respectively, as recommended by Werner and Brand (2001).

215 The parameters a<sub>12</sub>, b<sub>12</sub>, a<sub>13</sub>, and b<sub>13</sub> represent the slope and intercept of the calibration equations for <sup>12</sup>CH<sub>4</sub> and <sup>13</sup>CH<sub>4</sub>, respectively. They correct the instrument response and convert the raw isotopologue signals into calibrated mole fractions. The isotope ratio <sup>13</sup>r is calculated directly from the calibrated isotopologue mole fractions, and the total isotopologue normalization factor R<sub>sum</sub> accounts for all possible isotopic substitutions in CH<sub>4</sub>, including hydrogen-bearing species such as CH<sub>3</sub>D. An assumed δD value of–100% for atmospheric CH<sub>4</sub> was adopted from Quay et al. (1999). All calibrated values were reported on the WMO X2004A scale, and all isotopic ratios are reported relative to the VPDB (for δ<sup>13</sup>CH<sub>4</sub>) and VSMOW (for δD) international reference scales.

## 2.3.2 Delta-based calibration

225

The delta-based calibration approach corrects instrumental drift using  $\delta^{13}CH_4$  directly. A linear calibration is established using two reference gases with distinct  $\delta^{13}CH_4$  signatures as Eq. 8:

$$\delta^{13}CH_{4,cal} = a_{\delta} \times \delta^{13}CH_{4,drv} + b_{\delta} \tag{8}$$

Here,  $a_{\delta}$  and  $b_{\delta}$  represent the slope and intercept of the delta-based calibration, respectively, which

235





account for small systematic differences between the spectrometer-derived  $\delta^{13}CH_4$  values and the true isotopic compositions of the reference gases. These coefficients correct residual scale offsets and sensitivity deviations in the  $\delta^{13}CH_4$  retrievals before converting all measurements to the VPDB scale. This calibration is then applied to field observations, and  $\delta^{13}CH_4$  values are reported on the VPDB scale.

## 2.4 Correlation and statistics analysis

All statistical analyses were performed with a significance threshold of p < 0.05. Uncertainties were expressed as 95 % confidence intervals derived from bootstrap resampling. To assess the error characteristics, residuals and inter-method differences were visualized as histograms and fitted with Gaussian functions. The mean, standard deviation ( $\sigma$ ), RMSE, and MAE were computed to characterize the residual statistics. Gaussian functions were fitted to the histograms to examine whether the residuals followed a normal distribution.

#### 3. Results and Discussion

#### 3.1 Water vapor correction functions

240 We first performed laboratory experiments to quantify the water vapor effect on isotopologue mole fractions and δ<sup>13</sup>CH<sub>4</sub>. Reference gases with known CH<sub>4</sub> mole fractions and δ<sup>13</sup>CH<sub>4</sub> values were humidified to obtain varying H<sub>2</sub>O levels. The experiments revealed systematic dependencies of the <sup>12</sup>CH<sub>4</sub> and <sup>13</sup>CH<sub>4</sub> mole fractions and δ<sup>13</sup>CH<sub>4</sub>, on H<sub>2</sub>O concentrations (Fig. 3a-c).

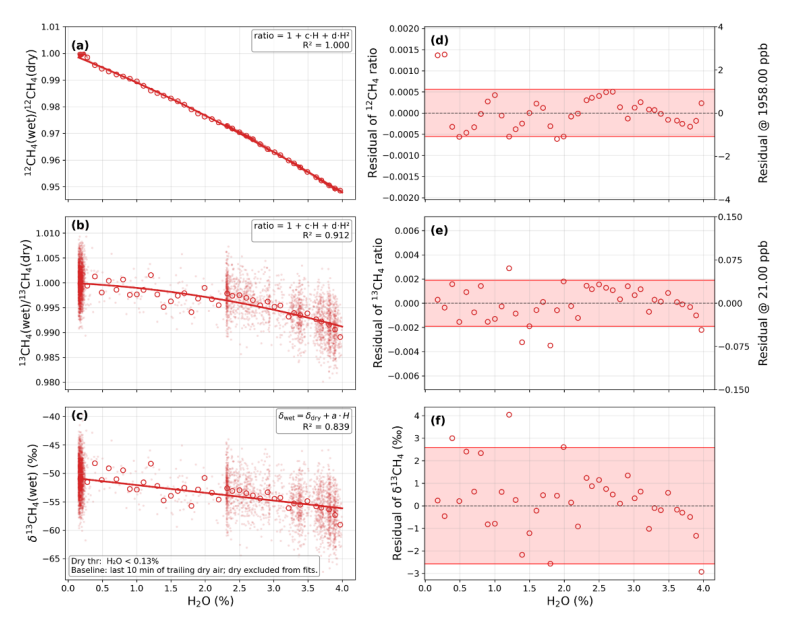


Fig.3 Water vapor correction functions for <sup>12</sup>CH<sub>4</sub>, <sup>13</sup>CH<sub>4</sub>, and δ<sup>13</sup>CH<sub>4</sub> derived from laboratory water vapor experiments (0.15–4.0% H<sub>2</sub>O). Panels a, b, and c show the fitted relationships between H<sub>2</sub>O concentration and the wet-to-dry ratios of <sup>12</sup>CH<sub>4</sub>, the wet-to-dry ratios of <sup>13</sup>CH<sub>4</sub>, and the δ<sup>13</sup>CH<sub>4</sub> deviation (δ<sup>13</sup>CH<sub>4</sub>, wet – δ<sup>13</sup>CH<sub>4</sub>, dry), respectively. Each open circle represents the mean value within a 0.1% H<sub>2</sub>O bin. The solid red lines indicate the best-

260

265

270

275

280





fit regression models (quadratic for  $^{12}$ CH<sub>4</sub> and  $^{13}$ CH<sub>4</sub>, linear for  $\delta^{13}$ CH<sub>4</sub>), and small points indicate raw observations. Panels d, e, and f show the corresponding residuals; the red shaded bands indicate the interval containing 90% of the data points, with parameters detailed in Table 3.

From these measurements, we established quadratic polynomial correction functions to describe the  $H_2O$  dependence of isotopologue mole fractions (Eqs.9-10), and derived an empirical linear function for  $\delta^{13}CH_4$  (Eq. 11). These relationships form the foundation for the water correction in field evaluations of calibration strategies (Section 3.3).

$$\frac{^{12}\text{CH}_{4,\text{wet}}}{^{12}\text{CH}_{4,\text{dry}}} = 1 - 0.0103 \times \text{H}_2\text{O} - 6.96 \times 10^{-4} \times (\text{H}_2\text{O})^2$$
(9)

$$\frac{^{13}\text{CH}_{4,\text{wet}}}{^{13}\text{CH}_{4,\text{dry}}} = 1 - 6.29 \times 10^{-4} \times \text{H}_2\text{O} - 3.94 \times 10^{-4} \times (\text{H}_2\text{O})^2$$
 (10)

$$\delta^{13}CH_{4, dry} = \delta^{13}CH_{4, wet} - 1.36 \times H_2O$$
 (11)

Here, the 'wet' mole fractions represent values observed from the humidified reference gas in laboratory conditions, while the 'dry' values correspond to the instrument-measured dry baseline. The baseline was obtained from the low-humidity segment at the end of the experiment ( $H_2O < 0.13\%$ ).  $H_2O$  denotes the water vapor concentration (%) directly measured by the analyzer (column " $H_2O$ "). For Eq. (9), the quadratic fit for  $^{12}CH_4$  is robust ( $R^2\approx1.000$ ), with fitted uncertainties of  $\pm1.2\times10^{-4}$  for the linear term and  $\pm3.9\times10^{-5}$  for the quadratic term. For Eq. (10), the quadratic dependence for  $^{13}CH_4$  is also significant ( $R^2\approx0.912$ ), and the fitted uncertainties are  $\pm3.8\times10^{-4}$  and  $\pm1.2\times10^{-4}$  for the linear and quadratic terms, respectively. For Eq. (11),  $\delta^{13}CH_4$ , wet exhibits a linear dependence on water vapor concentration, deviating from the dry reference  $\delta^{13}CH_4$ , dry by  $-1.36\pm0.10$  % per %  $H_2O$  ( $R^2\approx0.839$ ).

Table 3. Summary statistics of water vapor correction residuals for <sup>12</sup>CH<sub>4</sub>, <sup>13</sup>CH<sub>4</sub>, and δ<sup>13</sup>CH<sub>4</sub>.

Parameter	Baseline	Min	Median	80th percentile	90th percentile	Max	RMS
<sup>12</sup> CH <sub>4</sub>	1957.95 ppb	0.0034	0.5022	0.9346	1.0921	2.7090	0.8577
<sup>13</sup> CH <sub>4</sub>	20.84 ppb	0.0019	0.0213	0.0325	0.0413	0.0734	0.0288
$\delta^{13}CH_4$	-48.14 ‰	0.0970	0.6297	1.6761	2.5786	4.0386	1.4215

Note: Residuals were calculated as the absolute difference between binned means and fitted values from the water vapor correction functions for the experiment (0.15–4.0 %  $H_2O$ ). Reported statistics include minimum (Min), median, 80th and 90th percentile (80th percentile and 90th percentile), maximum (Max), and Root Mean Square (RMS) residuals. Percentile metrics (P80, P90) are used to represent the typical residual range while minimizing the influence of a few extreme humid points. All values are absolute residuals;  $^{12}CH_4$  and  $^{13}CH_4$  are in ppb, and  $\delta^{13}CH_4$  in %.

The residual statistics of the fitted water vapor correction functions are shown in Fig.3d-f, and detailed summarized in Table 3. The absolute residuals between the binned means and the fitted values were mostly small, confirming that the empirical corrections effectively capture the water vapor dependencies within 0.15–4.0 %  $\rm H_2O$ . For  $^{12}\rm CH_4$ , 80 % of the absolute residuals were below 0.93 ppb and 90 % below 1.09 ppb, corresponding to less than 0.05 % of the  $^{12}\rm CH_4$  reference concentration. The  $^{13}\rm CH_4$  residuals were similarly low, with 80 % and 90 % below 0.033 and 0.041 ppb (median = 0.021 ppb, RMS = 0.029 ppb). For  $\delta^{13}\rm CH_4$ , the median and 80th percentile residuals were 0.63 % and 1.68 %, respectively. Both  $^{12}\rm CH_4$  and  $^{13}\rm CH_4$  required quadratic correction functions to accurately describe the nonlinear response to

290

295

300





water vapor, reflecting the combined influence of dilution and pressure-broadening effects on observed absorption peak heights. This nonlinear behavior is consistent with previous characterizations of CRDS instruments (Chen et al., 2010; Wen et al., 2013; Griffith, 2018).

For  $^{12}$ CH<sub>4</sub>, the fitted coefficients (-0.0103 for the linear and  $-6.96 \times 10^{-4}$  for the quadratic term) closely match those reported by Chen et al. (2010) for bulk CH<sub>4</sub>, confirming the reproducibility of the water vapor interference across different analyzer models and laboratory setups. For  $^{13}$ CH<sub>4</sub>, the same quadratic correction was applied. Although the absolute residuals are small (80th percentile = 0.033 ppb), the fractional deviation is larger than for  $^{12}$ CH<sub>4</sub> because the  $^{13}$ CH<sub>4</sub> dry mole fraction is only  $\sim$ 21 ppb. Quantitatively, the 80th percentile residual corresponds to a relative uncertainty of approximately 0.15 % for  $^{13}$ CH<sub>4</sub>, compared with  $\sim$ 0.05 % for  $^{12}$ CH<sub>4</sub>, indicating that the  $^{13}$ CH<sub>4</sub> channel has about three times higher relative uncertainty. This suggests that the  $^{13}$ CH<sub>4</sub> signal is intrinsically more vulnerable to residual water bias. Because  $\delta^{13}$ CH<sub>4</sub> is derived from the ratio of  $^{13}$ CH<sub>4</sub> to  $^{12}$ CH<sub>4</sub>, any remaining humidity-dependent bias in  $^{13}$ CH<sub>4</sub> directly propagates into  $\delta^{13}$ CH<sub>4</sub>. In practice, this means that the accuracy of the isotopologue-specific calibration strategy under humid conditions is ultimately limited by the performance of the  $^{13}$ CH<sub>4</sub> water vaporcorrection.

By contrast,  $\delta^{13}$ CH<sub>4</sub> exhibited an approximately linear dependence on water vapor. This behavior arises because the nonlinear contributions in the numerator and denominator largely cancel when expressed as a ratio, leaving a dominant first-order term. This partial cancellation of nonlinear terms reflects the mathematical structure of  $\delta^{13}$ CH<sub>4</sub> as a ratio, where similar H<sub>2</sub>O dependencies in <sup>12</sup>CH<sub>4</sub> and <sup>13</sup>CH<sub>4</sub> tend to offset each other. Although the  $\delta^{13}$ CH<sub>4</sub>-H<sub>2</sub>O regression shows larger scatter than those for the individual isotopologues, the fitted slope of  $-1.36 \pm 0.10$  % %<sup>-1</sup> H<sub>2</sub>O over the full experimental range of 0.15 - 4.0 % H<sub>2</sub>O reflects enhanced sensitivity at higher humidity levels. When restricted to the same water vapor interval ( $\leq 1.5$  %), our fitted slope of  $-1.00 \pm 0.52$  % %<sup>-1</sup> H<sub>2</sub>O is not significantly different from the reported slope of  $-0.54 \pm 0.29$  % %<sup>-1</sup> H<sub>2</sub>O by Hoheisel et al. (2019).

305 It is worth noting that physical drying to approximately 0.1% H<sub>2</sub>O remains the recommended best practice for achieving sub-per-mil δ<sup>13</sup>CH<sub>4</sub> accuracy (e.g., Rella et al., 2015). In our study, the empirical water vapor correction functions were derived for the H<sub>2</sub>O range of 0.15–4.0%, which provide a complementary solution for measurements in humid air.

# 3.2 Comparison of $\delta^{13}CH_4$ calibration strategies for dry air sample measurements

310 For dry air sample measurements, both the isotopologue-specific and the delta-based calibration strategies yielded consistent δ¹³CH₄ results, with small and relatively stable offsets. For the certified target gas (Fig.4), both calibrated values were close to the assigned reference, with mean residuals of 0.15 ‰ for the isotopologue-specific method and 0.55 ‰ for the delta-based method. The inter-method difference (Δδ¹³CH₄ = iso − delta) averaged −0.40 ‰, indicating a slight but systematic offset toward lighter δ¹³C in the delta-based calibration. Residuals and differences followed approximately normal distributions, and their root-mean-square and mean absolute errors were both close to 2 ‰, comparable to the typical instrumental precision of the analyzer.

For measurements of air samples dried with the Nafion<sup>TM</sup> membrane dryer at the SORPES station (Fig. 5), both calibration schemes showed highly consistent  $\delta^{13}$ CH<sub>4</sub> retrievals. The two approaches yielded

325





overlapping daily means throughout DOY 240–280, with differences mostly within the  $1\sigma$  range of observational variability. The inter-method difference ( $\Delta\delta^{13}\mathrm{CH_4}$ ) averaged 0.29 ‰ and exhibited a near-Gaussian distribution ( $\sigma$  = 0.71 ‰), indicating minimal systematic bias between the two schemes for dried air sample measurements. A significant correlation between  $\Delta\delta^{13}\mathrm{CH_4}$  and CH<sub>4</sub> mole fraction ( $R^2$  = 0.97, p < 0.001) suggests that part of the residual offset may result from concentration-dependent effects of delta-based calibration. Although the ambient data showed slightly higher variability than laboratory measurements, both calibration methods remained stable and consistent across a wide range of CH<sub>4</sub> concentrations, demonstrating reliable performance for dried-air applications.

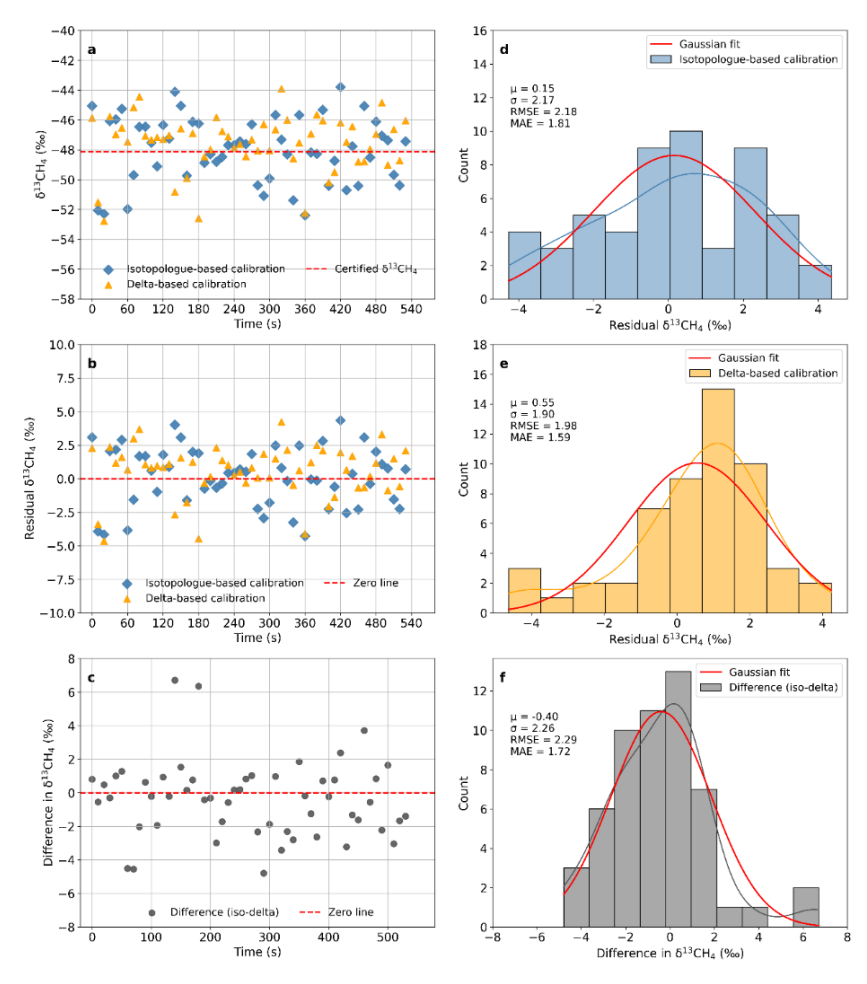


Fig. 4 Comparison of  $\delta^{13}\text{CH}_4$  calibration strategies for a dry reference gas. (a) Calibrated  $\delta^{13}\text{CH}_4$  from isotopologue-specific (blue diamonds) and delta-based (yellow triangles) strategies; the reference is shown as a red dashed line. (b) Residuals (calibrated – certified) for both strategies. (c) Time series of the difference between isotopologue-specific and delta-based calibrated  $\delta^{13}\text{CH}_4$  (hereafter referred to as the inter-method difference, iso – delta). (d, e) Histograms of residuals for the two strategies with Gaussian fits. (f) Distribution of the inter-method difference (iso – delta) with a Gaussian fit. For (d–f), Gaussian fits provide the mean ( $\mu$ ) and standard deviation ( $\sigma$ ), while root-mean-square error (RMSE) and mean absolute error (MAE) are computed from the data. All results are based on 10-s averaged data.

345





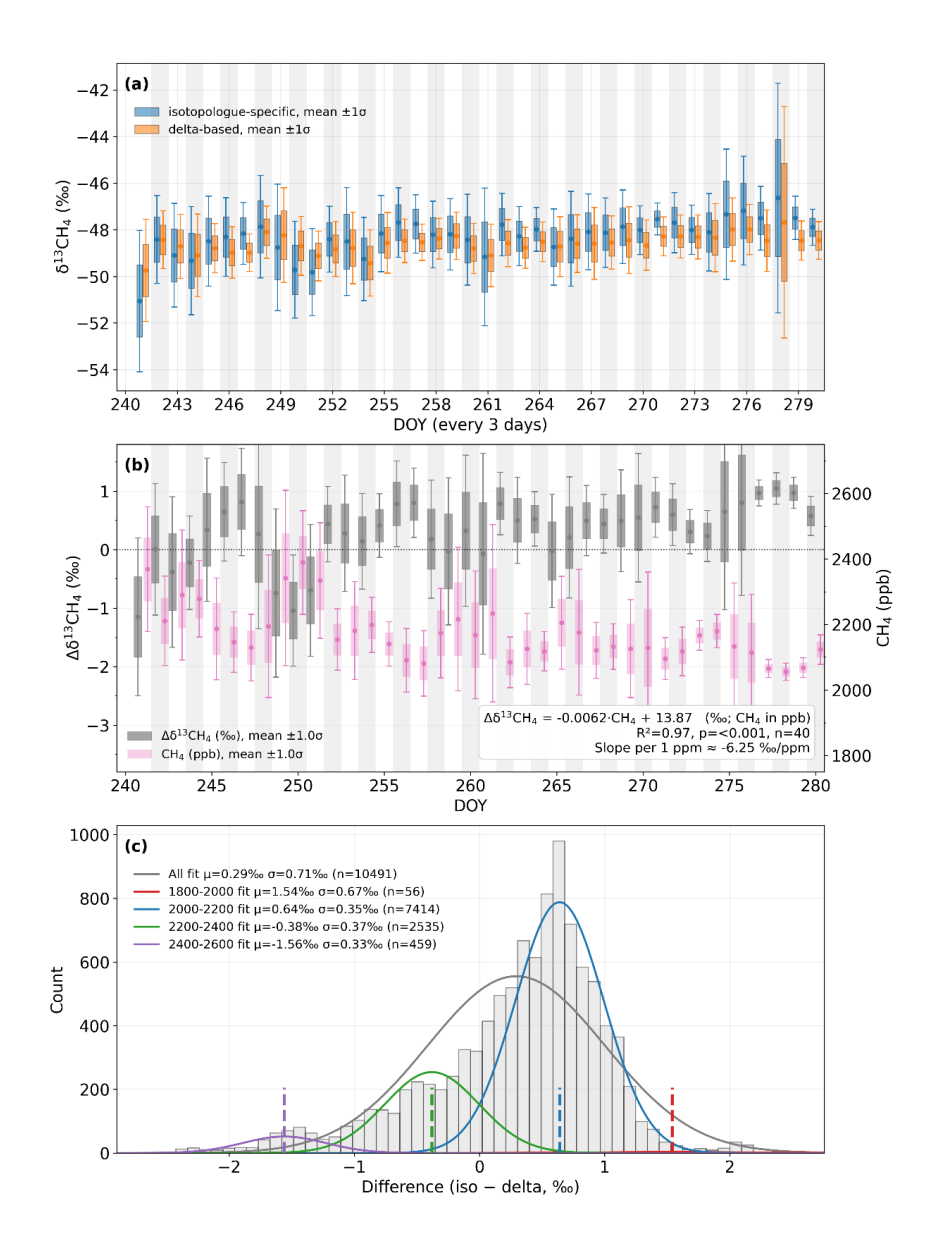


Fig.5 Comparison of  $\delta^{13}$ CH<sub>4</sub> calibration strategies at the SORPES station (dried ambient air, DOY 240–280, 2022). (a) Daily averaged  $\delta^{13}$ CH<sub>4</sub> values from isotopologue-specific (blue) and delta-based (orange) calibration strategies, with 1 $\sigma$  standard deviations. (b) Time series of the inter-method difference  $\Delta\delta^{13}$ CH<sub>4</sub> (iso – delta, grey bars) and corresponding CH<sub>4</sub> mole fraction (pink bars, right axis). The linear relationship between  $\Delta\delta^{13}$ CH<sub>4</sub> and CH<sub>4</sub> is shown with a fitted regression. (c) Histogram of  $\Delta\delta^{13}$ CH<sub>4</sub> (iso – delta) for all data and for different CH<sub>4</sub> concentration ranges, each fitted with a Gaussian function. The fitted mean ( $\mu$ ) and standard deviation ( $\sigma$ ) are reported for each subset. All analyses are based on 5-min averaged data.

For dry air sample measurements, both calibration strategies yielded nearly identical  $\delta^{13}$ CH<sub>4</sub> results, indicating that the isotopic retrievals are consistent when water vapor interference is negligible. However, a strong correlation between the inter-method difference ( $\Delta\delta^{13}$ CH<sub>4</sub>) and CH<sub>4</sub> mole fraction (Fig.5b)

365

370

375

380

385





suggests that concentration-dependent effects may still influence the delta-based calibration.

Although the present dataset cannot explicitly isolate the cause, this pattern agrees well with the theoretical framework of Griffith et al. (2012), which demonstrated that non-zero intercepts and nonlinearities in isotopologue calibrations inevitably propagate into δ<sup>13</sup>C space, producing apparent δ<sup>13</sup>C-concentration coupling. Griffith (2018) further generalized this analysis, identifying both inverse and linear dependencies of δ<sup>13</sup>CH<sub>4</sub> on CH<sub>4</sub> concentration. Our results exhibit the concentration-dependent behavior predicted by these studies. Similar dependencies have also been reported for CO<sub>2</sub> isotope measurements (Wen et al., 2013; Pang et al., 2016; Braden-Behrens et al., 2017), indicating that such effects are intrinsic to δ<sup>13</sup>C-based formulations rather than instrument-specific anomalies. Beyond the dry air regime examined here, additional deviations may emerge in humid air, where spectral interference becomes a dominant factor influencing isotopic accuracy.

To further assess the robustness of these correction functions under realistic environmental conditions, we examined their performance in humidified air samples at the rice paddy site.

#### 3.3 Performance of calibration strategies under humid air conditions

To evaluate the performance of the water vapor correction under field conditions, both calibration strategies were applied to a humidified target gas at the rice paddy site (DOY 240–280, 2018). As shown in Fig. 6, after applying the correction functions, both isotopologue-specific and delta-based calibrations reproduced  $\delta^{13}\text{CH}_4$  values close to the certified reference (Fig. 6a), confirming that the equations effectively removed humidity-induced artifacts. The isotopologue-specific calibration yields  $\delta^{13}\text{CH}_4$  values that align more tightly with the reference, while the delta-based calibrated results retain a small positive offset (Fig. 6a–c). Consistent with the histograms, the isotopologue-specific residuals improved from  $\mu = -0.84\%$  ( $\sigma = 0.30\%$ ) before correction to  $\mu = -0.31\%$  ( $\sigma = 0.24\%$ ) after correction. In contrast, the delta-based residuals remained consistently near +0.5% both before and after correction ( $\mu \approx +0.48$  to +0.49%,  $\sigma = 0.26\%$ ; Fig. 6d–e). The inter-method difference (iso – delta) has a mean of –0.80% after correction with a reduced spread ( $\sigma = 0.14\%$ ; Fig. 6f), indicating a stable, strategy-dependent offset. These results confirm that the correction equations effectively mitigate humidity-induced artifacts, particularly for the isotopologue-specific approach, providing a reliable basis for subsequent field

The Jurong site represents a typical rice paddy ecosystem, characterized by persistently high ambient humidity and strong methane emissions. During the observation period,  $H_2O$  concentrations frequently exceeded 3%, while  $CH_4$  mole fractions varied substantially, ranging from background levels below 2000 ppb to episodic peaks above 5000 ppb. These conditions provide a stringent test for calibration strategies, as both elevated humidity and broad concentration ranges can amplify systematic biases in  $\delta^{13}CH_4$  retrievals.

Fig. 7 illustrates the contrasting behavior of isotopologue-specific and delta-based calibrations for humid air observations. Daily mean  $\delta^{13}$ CH<sub>4</sub> values from the delta-based calibration were consistently offset relative to those from the isotopologue-specific approach, and exhibit greater variability (Fig. 7a). The inter-method difference,  $\Delta\delta^{13}$ CH<sub>4</sub> (iso – delta), closely tracked temporal variations in both H<sub>2</sub>O and CH<sub>4</sub> mole fractions (Fig. 6b), showing significant correlations (R<sup>2</sup> = 0.48 with H<sub>2</sub>O and R<sup>2</sup> = 0.75 with CH<sub>4</sub>;

395

400





p < 0.001). This bias was strongly concentration-dependent, with  $\Delta\delta^{13}$ CH<sub>4</sub> shifting from approximately -10.0 to -1.3 % at CH<sub>4</sub> < 3500 ppb to +1.6 to +9.0 % at CH<sub>4</sub> > 3500 ppb (Fig. 7c).

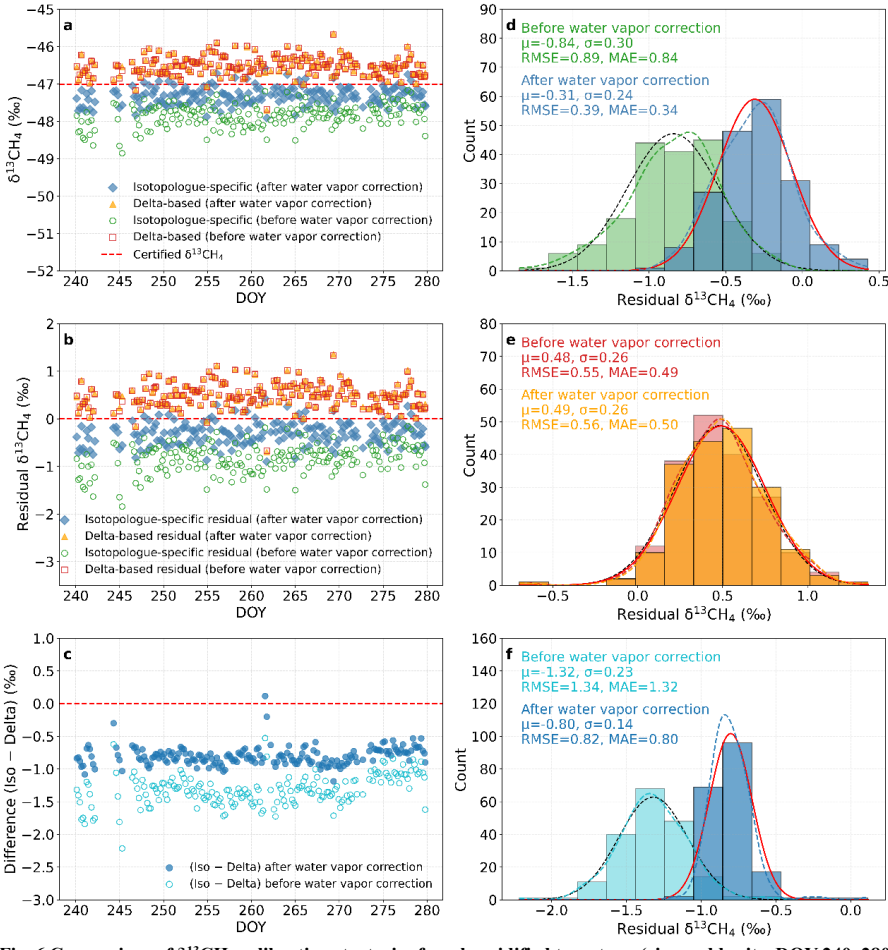


Fig. 6 Comparison of  $\delta^{13}\text{CH}_4$  calibration strategies for a humidified target gas (rice paddy site, DOY 240–280, 2018). (a)  $\delta^{13}\text{CH}_4$  values from the isotopologue-specific (blue diamonds) and delta-based (orange triangles) calibrations, shown both before (open symbols) and after (filled symbols) applying the water vapor correction. The certified reference value is indicated by the red dashed line. (b) Residuals (calibrated – certified) for both calibration strategies, with open and filled markers representing results before and after water vapor correction, respectively. (c) Time series of the inter-method difference  $\Delta\delta^{13}\text{CH}_4$  = (iso – delta), shown before (open) and after (filled) water vapor correction. (d, e) Histograms of residuals for the two calibration strategies before and after water vapor correction, with Gaussian fits illustrating their respective distributions. (f) Histogram of the inter-method difference (iso – delta) before and after water vapor correction, also fitted with Gaussian functions. For panels (d–f), Gaussian fits provide the mean (µ) and standard deviation ( $\sigma$ ), while the root-mean-square error (RMSE) and mean absolute error (MAE) are calculated from the data. All results are based on 5-min averaged measurements after applying the empirical water vapor correction equations functions.





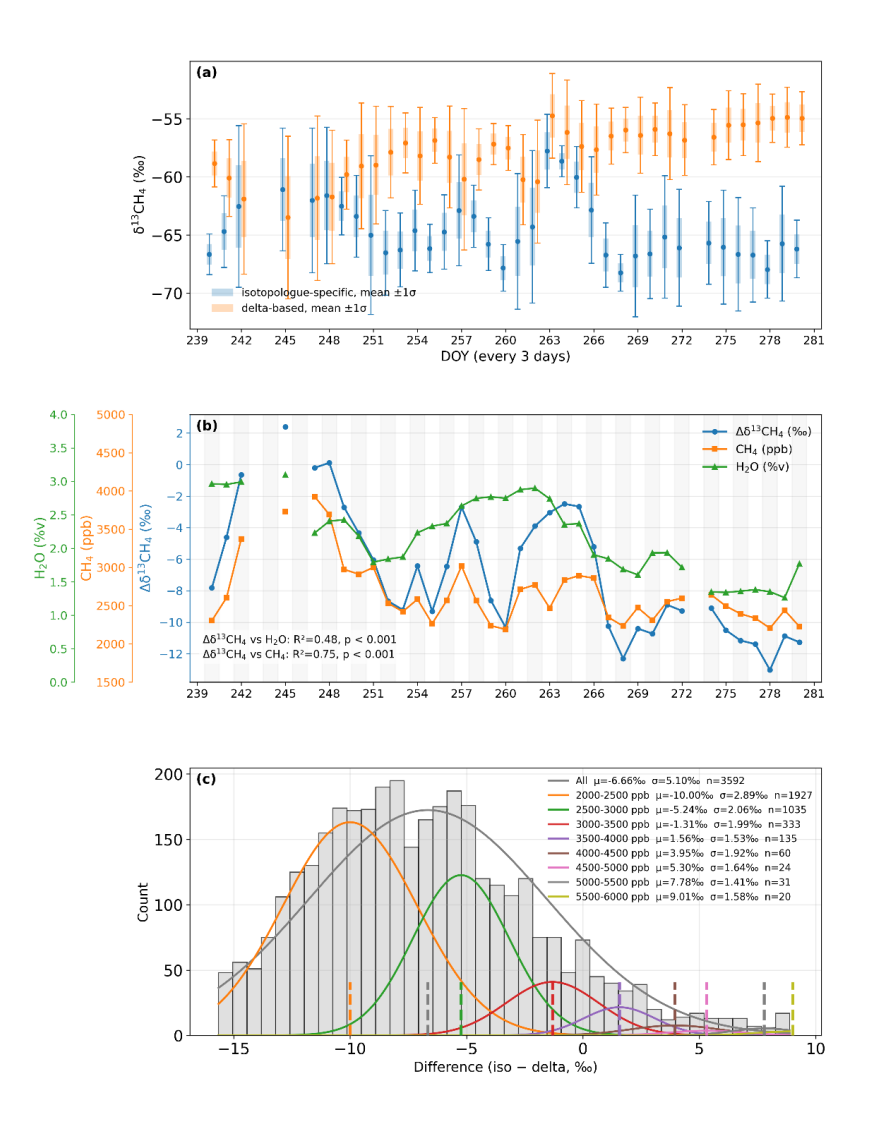


Fig. 7. Field comparison of  $\delta^{13}$ CH<sub>4</sub> calibration strategies for humid air observations at the rice paddy site (DOY 240–280, 2018). (a) Daily mean  $\delta^{13}$ CH<sub>4</sub> from isotopologue-specific (blue) and delta-based (orange) calibrations (mean  $\pm$  1 $\sigma$ ). (b) Time series of the inter-method difference  $\delta^{13}$ CH<sub>4</sub> (iso – delta, blue line) together with total CH<sub>4</sub> mole fraction (orange line) and H<sub>2</sub>O concentration (green line). (c) Histogram of  $\delta^{13}$ CH<sub>4</sub> differences (iso – delta) grouped by CH<sub>4</sub> mole-fraction ranges, each fitted with a Gaussian function. The fitted mean ( $\mu$ ) and standard deviation ( $\sigma$ ) are reported for each subset. All results are based on 5-min averages.

410 These results highlight that high humidity and large CH<sub>4</sub> variability exacerbate the intrinsic weaknesses of delta-based calibration, consistent with earlier observations for CO<sub>2</sub> isotopes (Wen et al., 2013; Pang et al., 2016). Without explicit correction, such biases can propagate into source signature retrievals, leading to systematic offsets in rice-paddy plume analyses. Although a significant correlation between Δδ<sup>13</sup>CH<sub>4</sub> and H<sub>2</sub>O was observed, this may not directly represent a direct spectroscopic effect of water vapor. At the Jurong site, episodes of high humidity often coincided with strong CH<sub>4</sub> emissions,

435

440

445

450





producing an intrinsic covariance between  $H_2O$  and  $CH_4$ . Consequently, part of the apparent  $\Delta\delta^{13}CH_4$ — $H_2O$  relationship may arise from this co-variation rather than from water vapor interference alone. The empirical correction functions used here effectively capture the dominant humidity effects at the isotopologue level, but may not fully account for additional spectral interferences associated with pressure or temperature variability. It should also be emphasized that, in practice, physical drying of air samples remains the preferred approach, whereas empirical water vapor corrections should serve only as a secondary option when drying is not feasible. Addressing these aspects in future work will further refine calibration strategies and enhance their applicability across diverse environments.

#### 3.4 Application of calibration strategies in field observations

To further quantify the relationship between the inter-method bias (Δδ¹³CH₄) and CH₄ concentration, we regressed Δδ¹³CH₄ against CH₄ mole fraction using the expression Δδ¹³CH₄ = c₀ + c₁/CH₄ + c₂×CH₄ following Griffith et al 2018 (Table 4). At both field sites, most data points are concentrated within a relatively narrow CH₄ range, representing the dominant concentration regimes during field observations: 2000–3000 ppb at Jurong and 2000–2500 ppb at SORPES. These ranges capture the typical operational conditions under which calibration biases are most relevant.

At the Jurong site,  $\Delta\delta^{13}$ CH<sub>4</sub> exhibited a pronounced 1/CH<sub>4</sub> dependence, with significantly negative  $c_1$  terms (p < 0.01) and negligible  $c_2$  values. This pattern indicates that the inter-method difference increases toward lower CH<sub>4</sub> concentrations, where signal dilution and pressure-broadening effects become more influential. Although the water vapor correction successfully mitigates first-order humidity effects, the remaining dependence likely arises from the coupled response of isotopologue scaling and dilution to varying CH<sub>4</sub> and H<sub>2</sub>O levels. At the SORPES site,  $\Delta\delta^{13}$ CH<sub>4</sub> was better characterized by the CH<sub>4</sub> (c<sub>2</sub>) term, showing a weak but positive dependence on concentration (c<sub>2</sub> > 0, p < 0.05). In the absence of strong humidity effects, the difference between isotopologue-specific and delta-based calibrations thus reflects higher-order nonlinearities intrinsic to the delta-based formulation. The contrasting dominant terms between Jurong and SORPES highlight how humidity modulates the expression of calibration nonlinearity: humid air amplifies inverse (1/CH<sub>4</sub>) dependencies, whereas dry air emphasizes minor linear (CH<sub>4</sub>) effects.

These site-specific regressions are consistent with the theoretical framework proposed by Griffith (2018), where the inverse (1/CH<sub>4</sub>) and linear (CH<sub>4</sub>) terms correspond to intercept-driven and quadratic nonlinearities, respectively. The slope variations observed in Fig. 7c further support this interpretation, providing a mechanistic explanation for the site-dependent discrepancies in Figs. 6–7. However, despite the effectiveness of the water vapor correction functions across the full humidity range, the residual concentration dependence of  $\Delta\delta^{13}$ CH<sub>4</sub> suggests that both CH<sub>4</sub> and H<sub>2</sub>O jointly modulate the inter-method bias, with their relative contributions differing between humid and dry air. In practice, field measurements typically include an air-drying stage (e.g., Nafion<sup>TM</sup> membrane dryers), but physical drying alone cannot fully remove water vapor interference. Even well-maintained Nafion<sup>TM</sup> systems leave residual H<sub>2</sub>O at 0.3–0.6 % under ambient conditions—enough to bias  $\delta^{13}$ CH<sub>4</sub> retrievals, particularly at humid sites or during high-CH<sub>4</sub> events. Therefore, an explicit H<sub>2</sub>O correction remains necessary rather than assuming that drying alone ensures isotopic accuracy (Welp et al., 2013; Paul et al., 2020).

https://doi.org/10.5194/egusphere-2025-5569 Preprint. Discussion started: 19 November 2025 © Author(s) 2025. CC BY 4.0 License.





Overall, these site-specific behaviors provide practical guidance for field deployment. Under well-dried conditions with relatively stable CH<sub>4</sub> mole fractions (e.g., SORPES), the residual difference between the isotopologue-specific and delta-based calibrations is small, dominated by weak high-concentration nonlinearities, and can be characterized empirically. In such cases, the delta-based approach remains operationally acceptable for routine monitoring. By contrast, for humid air, high-emission conditions with large CH<sub>4</sub> variability (e.g., Jurong), the inter-method bias exhibits a strong inverse-concentration dependence and should not be treated as a constant offset. In these environments, the isotopologue-specific calibration is required to avoid systematic shifts in inferred source signatures. In practice, physical drying of the sample air should remain the primary strategy wherever feasible, and the combination of humidity correction and isotopologue-specific calibration should be considered the default fallback when effective drying cannot be maintained.





Table.4 Regression results of concentration dependence of  $\Delta\delta^{13}$ CH<sub>4</sub> at Jurong (humid air) and SORPES (dry air) sites.  $\Delta\delta^{13}$ CH<sub>4</sub> is defined as the inter-method difference between isotopologue-specific and delta-based calibrated  $\delta^{13}$ CH<sub>4</sub> ( $\Delta=\delta^{13}$ CH<sub>4</sub> is  $-\delta^{13}$ CH<sub>4</sub> delta). The dependence on CH<sub>4</sub> mole fraction was fitted using the function  $\Delta=c_0+c_1$ CH<sub>4</sub> +  $c_2$ CH<sub>4</sub>, where  $c_0$ ,  $c_1$ , and  $c_2$  are regression coefficients (Griffih et al., 2018). All results are based on 5-min averaged data. Significance levels: p < 0.05 (\*\*), p < 0.01 (\*\*). The "Dominant term" column identifies whether the contribution of  $c_1$  or  $c_2$  is greater, based on their evaluated magnitudes at the median CH<sub>4</sub> mole fraction of each concentration range.

Site, CH <sub>4</sub> mole fraction (ppb, % of	Water	R	Regression coefficients (co, c1, c2)	0, C1, C2)	Fit statistics	Number of data Dominant	Dominan
data)	(H <sub>2</sub> O, %)	c0	c1(1/CH <sub>4</sub> , ppb)	c2(CH4, ppb)	$(\mathbb{R}^2, p)$	points (N)	term
Jurong, 2000 - 6000 (100%)		24.84	$-7.61 \times 10^4$	-6.45×10 <sup>-4</sup>	0.86**	3565	c1, 1/CH <sub>4</sub>
Jurong, 2000 - 2500 (54.05%)	Humid air:	146.63	-2.26×10 <sup>5</sup>	-0.0251	0.66**	1927	c1, 1/CH <sub>4</sub>
Jurong, 2500 - 3000 (29.03%)	(1.0%~3.5%)	-34.57	$1.75 \times 10^4$	0.0084	0.18	1035	c2, CH <sub>4</sub>
Jurong, 3000 - 3500 (9.34%)		156.22	$-2.96 \times 10^{5}$	-0.0203	0.34	333	c1, 1/CH
SORPES, 1800 - 3000 (100%)		-15.08	$3.33 \times 10^4$	$7.46 \times 10^{-5}$	0.78**	35629	c1, CH4
SORPES, 1500 - 2000 (3.08%)	Dried air:	67.52	$-5.09 \times 10^4$	-0.0199	0.07	1100	c2, CH4
SORPES, 2000 -2500 (93.86%)	(<0.1%)	1.57	$1.42 \times 10^4$	-0.0035	0.73**	33442	c2, CH <sub>4</sub>
SORPES, 2500 -3000 (3.05%)		-9.05	$2.42 \times 10^{4}$	-0.0009	0.66**	1087	cl. 1/CH <sub>4</sub>





#### 4 Conclusions

470

475

480

485

We evaluated two  $\delta^{13}$ CH<sub>4</sub> calibration strategies, delta-based and isotopologue-specific calibration, using a Picarro G2201-i isotopic analyzer under both laboratory and field conditions. Empirical water vapor correction functions were established based on laboratory experiments (0.15–4.0 % H<sub>2</sub>O) to effectively remove humidity-induced biases in isotopologue mole fractions and  $\delta^{13}$ CH<sub>4</sub>. The observed water vapor dependencies were best represented by quadratic functions for  $^{12}$ CH<sub>4</sub> and  $^{13}$ CH<sub>4</sub>, and a linear function for  $\delta^{13}$ CH<sub>4</sub>. For  $^{12}$ CH<sub>4</sub> and  $^{13}$ CH<sub>4</sub>, the residuals fell within the analyzer's precision, while  $\delta^{13}$ CH<sub>4</sub> residuals remained small and comparable to the precision. These water correction equations provide a robust basis for correcting field data. While most field systems employ physical air drying (e.g., Nafion<sup>TM</sup> dryers), residual H<sub>2</sub>O often persists at levels sufficient to introduce measurable isotopic bias. Therefore, explicit humidity correction remains necessary, particularly under high-humidity conditions.

For dry air measurements, both calibration strategies yielded consistent  $\delta^{13}CH_4$  results. Laboratory tests and dried-air observations at the SORPES site confirmed nearly identical retrievals between the two approaches, with only minor offsets ( $\Delta\delta^{13}CH_4\approx0.29$  %) and concentration dependencies within the analytical uncertainty. In contrast, significant inter-method discrepancies emerged for humid air measurement. The bias ( $\Delta\delta^{13}CH_4$ ) correlated strongly with both  $CH_4$  and  $H_2O$  levels, indicating that humidity and concentration jointly modulate calibration accuracy. Consequently, the isotopologue-specific calibration method is better suited for accurate  $\delta^{13}CH_4$  retrievals under conditions of fluctuating humidity and  $CH_4$  concentrations.

In conclusion, the combination of isotopologue-specific calibration and empirical water vapor correction provides a reliable and transferable framework for precise  $\delta^{13}CH_4$  measurements in both dry and humid air.

Author contributions. J.L. and H.C. conceived the study. J.L. performed the laboratory and field experiments, analyzed the data. X.C. and A.D., W.J., Y.Z., and J.C. provided scientific guidance for the field experiments. J.L. and H.C. wrote the manuscript with contributions from all authors.

Acknowledgements. The study was supported by the National Natural Science Foundation of China (grant numbers 42305129, 42475115, U24A20590), the Fundamental Research Funds for the Central Universities - Cemac "GeoX" Interdisciplinary Program (grant numbers 2024QNXZ01, 2024300245, 14380235). This work was supported by the project of Youth Crossdisciplinary Team of the Chinese

Academy of Sciences (No. 2023000126). This research was also supported by the Collaborative Innovation Center of Climate Change, Jiangsu Province.

Data availability. the data used in this study are available from the corresponding author upon reasonable request.

500





#### Reference

505

510

515

- Bakkaloglu, S., Lowry, D., Fisher, R. E., Menoud, M., Lanoisellé, M., Chen, H., Röckmann, T., and Nisbet, E. G.: Stable isotopic signatures of methane from waste sources through atmospheric measurements, Atmospheric Environment, 276, 119021, 2022, https://doi.org/10.1016/j.atmosenv.2022.119021
- Berden, G. and Engeln, R.: Cavity ring-down spectroscopy: techniques and applications, John Wiley & Sons, 2009, <a href="https://doi.org/10.1002/9781444308259">https://doi.org/10.1002/9781444308259</a>
- Braden-Behrens, J., Yan, Y., and Knohl, A.: A new instrument for stable isotope measurements of <sup>13</sup>C and <sup>18</sup>O in CO<sub>2</sub> instrument performance and ecological application of the Delta Ray IRIS analyzer, Atmospheric Measurement Techniques, 10, 4537–4560, 2017, <a href="https://doi.org/10.5194/amt-10-4537-2017">https://doi.org/10.5194/amt-10-4537-2017</a>
- Chen, H., Winderlich, J., Gerbig, C., Hoefer, A., Rella, C., Crosson, E., Van Pelt, A., Steinbach, J., Kolle, O., and Beck, V.: High-accuracy continuous airborne measurements of greenhouse gases (CO<sub>2</sub> and CH<sub>4</sub>) using the cavity ring-down spectroscopy (CRDS) technique, Atmospheric Measurement Techniques, 3, 375–386, 2010, <a href="https://doi.org/10.5194/amt-3-375-2010">https://doi.org/10.5194/amt-3-375-2010</a>
- Crosson, E.: A cavity ring-down analyzer for measuring atmospheric levels of methane, carbon dioxide, and water vapor, Applied Physics B, 92, 403–408, 2008, <a href="https://doi.org/10.1007/s00340-008-3135-y">https://doi.org/10.1007/s00340-008-3135-y</a>
- Crosson, E. R., Ricci, K. N., Richman, B. A., Chilese, F. C., Owano, T. G., Provencal, R. A., Todd, M. W., Glasser, J., Kachanov, A. A., and Paldus, B. A.: Stable isotope ratios using cavity ring-down spectroscopy: determination of \(^{13}\)C/\(^{12}\)C for carbon dioxide in human breath, Analytical Chemistry, 74, 2003–2007, 2002, \(\frac{https:\/\doi.org/10.1021/ac025511d\)
  - De Groot, P. A.: Handbook of stable isotope analytical techniques, Elsevier, 2004, https://www.sciencedirect.com/science/book/9780444511140
- 525 Defratyka, S. M., France, J. L., Fisher, R. E., Lowry, D., Fernandez, J. M., Bakkaloglu, S., Yver-Kwok, C., Paris, J.-D., Bousquet, P., and Arnold, T.: Evaluation of data processing strategies for methane isotopic signatures determined during near-source measurements, Tellus B: Chemical and Physical Meteorology, 77, 2025, <a href="https://doi.org/10.16993/tellusb.1878">https://doi.org/10.16993/tellusb.1878</a>
- Ding, A., Nie, W., Huang, X., Chi, X., Sun, J., Kerminen, V.-M., Xu, Z., Guo, W., Petäjä, T., and Yang, X.: Long-term observation of air pollution—weather/climate interactions at the SORPES station: a review and outlook, Frontiers of Environmental Science & Engineering, 10, 1–15, 2016, <a href="https://doi.org/10.5194/acp-19-11791-2019">https://doi.org/10.5194/acp-19-11791-2019</a>
  - Ehleringer, J. R. and Osmond, C. B.: Stable isotopes, in: Plant physiological ecology: field methods and instrumentation, Springer, 281–300, 1989, <a href="https://doi.org/10.1007/978-94-009-2221-1">https://doi.org/10.1007/978-94-009-2221-1</a>
- Flores, E., Viallon, J., Moussay, P., Griffith, D. W., and Wielgosz, R. I.: Calibration strategies for FT-IR and other isotope ratio infrared spectrometer instruments for accurate δ¹³C and δ¹³O measurements of CO₂ in air, Analytical Chemistry, 89, 3648–3655, 2017, <a href="https://doi.org/10.1021/acs.analchem.6b05063">https://doi.org/10.1021/acs.analchem.6b05063</a>
- Forster, P., Storelvmo, T., Armour, K., Collins, W., Dufresne, J.-L., Frame, D., Lunt, D., Mauritsen, T.,
  Palmer, M., and Watanabe, M.: The Earth's energy budget, climate feedbacks, and climate sensitivity,
  2021, <a href="https://doi.org/10.1017/9781009157896.009">https://doi.org/10.1017/9781009157896.009</a>
  - France, J. L., Fisher, R. E., Lowry, D., Allen, G., Andrade, M. F., Bauguitte, S. J.-B., Bower, K., Broderick, T. J., Daly, M. C., and Forster, G.: δ<sup>13</sup>C methane source signatures from tropical wetland and rice field emissions, Philosophical Transactions of the Royal Society A, 380, 20200449, 2022, <a href="https://doi.org/10.1098/rsta.2020.0449">https://doi.org/10.1098/rsta.2020.0449</a>
  - Griffith, D., Deutscher, N., Caldow, C., Kettlewell, G., Riggenbach, M., and Hammer, S.: A Fourier transform infrared trace gas and isotope analyser for atmospheric applications, Atmospheric Measurement Techniques, 5, 2481–2498, 2012, https://doi.org/10.5194/amt-5-2481-2012
- Griffith, D. W.: Calibration of isotopologue-specific optical trace gas analysers: a practical guide,
  Atmospheric Measurement Techniques, 11, 6189–6201, 2018, <a href="https://doi.org/10.5194/amt-11-6189-2018">https://doi.org/10.5194/amt-11-6189-2018</a>
  - Hoheisel, A., Yeman, C., Dinger, F., Eckhardt, H., and Schmidt, M.: An improved method for mobile characterisation of  $\delta^{13}\text{CH}_4$  source signatures and its application in Germany, Atmospheric Measurement Techniques, 12, 1123–1139, 2019, <a href="https://doi.org/10.5194/amt-12-1123-2019">https://doi.org/10.5194/amt-12-1123-2019</a>
- IAEA: Measurement of the stable carbon isotope ratio in atmospheric CH<sub>4</sub> using laser spectroscopy for CH<sub>4</sub> source characterization, International Atomic Energy Agency, 2024, https://doi.org/10.61092/iaea.logm-wiux
  - IPCC: Climate Change 2007: The Physical Science Basis. Contribution of Working Group I to the Fourth Assessment Report of the Intergovernmental Panel on Climate Change, Cambridge University Press,

580

595

600

605





- 560 Cambridge, United Kingdom and New York, NY, USA, 996 pp., 2007, https://wedocs.unep.org/20.500.11822/30763
  - Kirschke, S., Bousquet, P., Ciais, P., Saunois, M., Canadell, J. G., Dlugokencky, E. J., Bergamaschi, P., Bergmann, D., Blake, D. R., and Bruhwiler, L.: Three decades of global methane sources and sinks, Nature Geoscience, 6, 813–823, 2013, <a href="https://doi.org/10.1038/ngeo1955">https://doi.org/10.1038/ngeo1955</a>
- 565 Lan, X., Basu, S., Schwietzke, S., Bruhwiler, L. M., Dlugokencky, E. J., Michel, S. E., Sherwood, O. A., Tans, P. P., Thoning, K., and Etiope, G.: Improved constraints on global methane emissions and sinks using δ13CH4, Global Biogeochemical Cycles, 35, e2021GB007000, 2021, https://doi.org/10.1029/2021GB007000
- Levin, I., Bergamaschi, P., Dörr, H., and Trapp, D.: Stable isotopic signature of methane from major sources in Germany, Chemosphere, 26, 161–177, 1993, <a href="https://doi.org/10.1016/0045-6535(93)90419-6">https://doi.org/10.1016/0045-6535(93)90419-6</a>
  - Li, J., Zhang, Y., Gu, L., Li, Z., Li, J., Zhang, Q., Zhang, Z., and Song, L.: Seasonal variations in the relationship between sun-induced chlorophyll fluorescence and photosynthetic capacity from the leaf to canopy level in a rice crop, Journal of Experimental Botany, 71, 7179–7197, 2020, https://doi.org/10.1093/jxb/eraa408
  - Miller, J. B., Mack, K. A., Dissly, R., White, J. W., Dlugokencky, E. J., and Tans, P. P.: Development of analytical methods and measurements of <sup>13</sup>C/<sup>12</sup>C in atmospheric CH4 from the NOAA Climate Monitoring and Diagnostics Laboratory global air sampling network, Journal of Geophysical Research: Atmospheres, 107, ACH 11–11–ACH 11–15, 2002, https://doi.org/10.1029/2001JD000630
  - Nisbet, E., Dlugokencky, E., Manning, M., Lowry, D., Fisher, R., France, J., Michel, S., Miller, J., White, J., and Vaughn, B.: Rising atmospheric methane: 2007–2014 growth and isotopic shift, Global Biogeochemical Cycles, 30, 1356–1370, 2016, <a href="https://doi.org/10.1002/2016gb005406">https://doi.org/10.1002/2016gb005406</a>
- Nisbet, E., Fisher, R., Lowry, D., France, J., Allen, G., Bakkaloglu, S., Broderick, T., Cain, M., Coleman,
  M., and Fernandez, J.: Methane mitigation: methods to reduce emissions, on the path to the Paris
  agreement, Reviews of Geophysics, 58, e2019RG000675, 2020,
  https://doi.org/10.1029/2019RG000675
  - Olivier, J. G. and Berdowski, J. J.: Global emission sources and sinks, in: The climate system, CRC Press, 33–77, 2021, <a href="https://doi.org/10.1201/9781003211266">https://doi.org/10.1201/9781003211266</a>
- Pang, J., Wen, X., Sun, X., and Huang, K.: Intercomparison of two cavity ring-down spectroscopy analyzers for atmospheric <sup>13</sup>CO<sub>2</sub>/<sup>12</sup>CO<sub>2</sub> measurement, Atmospheric Measurement Techniques, 9, 3879–3891, 2016, <a href="https://doi.org/10.5194/amt-9-3879-2016">https://doi.org/10.5194/amt-9-3879-2016</a>
  - Patra, P. K. and Khatri, P.: Atmospheric mixing ratio of greenhouse gases and radiative forcing, in: Handbook of Air Quality and Climate Change, Springer, 1–29, 2022, <a href="https://doi.org/10.1007/978-981-15-2527-8">https://doi.org/10.1007/978-981-15-2527-8</a> 29-1
  - Paul, D., Scheeren, H. A., Jansen, H. G., Kers, B. A. M., Miller, J. B., Crotwell, A. M., Michel, S. E., Gatti, L. V., Domingues, L. G., Correia, C. S. C., Neves, R. A. L., Meijer, H. A. J., and Peters, W.: Evaluation of a field-deployable Nafion-based air-drying system for collecting whole air samples and its application to stable isotope measurements of CO<sup>2</sup>, Atmospheric Measurement Techniques, 13, 4051–4064, 2020, <a href="https://doi.org/10.5194/amt-13-4051-2020">https://doi.org/10.5194/amt-13-4051-2020</a>
  - Picarro: Water vapor correction in CRDS isotopic measurements: G2101-i analyzer white paper, Picarro Inc., Santa Clara, CA, USA, 2012.
  - Quay, P., Stutsman, J., Wilbur, D., Snover, A., Dlugokencky, E., and Brown, T.: The isotopic composition of atmospheric methane, Global Biogeochemical Cycles, 13, 445–461, 1999, https://doi.org/10.1029/1998GB900006
  - Rella, C.: Accurate stable carbon isotope ratio measurements in humid gas streams using the Picarro  $\delta^{13}CO_2$  G2101-i gas analyzer, White Paper of Picarro Inc., 1–13, 2012.
  - Rella, C., Hoffnagle, J., He, Y., and Tajima, S.: Local- and regional-scale measurements of CH4, δ13CH4, and C2H6 in the Uintah Basin using a mobile stable isotope analyzer, Atmospheric Measurement Techniques, 8, 4539–4559, 2015, <a href="https://doi.org/10.5194/amt-8-4539-2015">https://doi.org/10.5194/amt-8-4539-2015</a>
  - Rella, C. W., Chen, H., Andrews, A. E., Filges, A., Gerbig, C., Hatakka, J., Karion, A., Miles, N. L., Richardson, S. J., and Steinbacher, M.: High accuracy measurements of dry mole fractions of carbon dioxide and methane in humid air, Atmospheric Measurement Techniques, 6, 837–860, 2013, https://doi.org/10.5194/amt-6-837-2013
- Rice, A. L., Butenhoff, C. L., Teama, D. G., Röger, F. H., Khalil, M. A. K., and Rasmussen, R. A.: Atmospheric methane isotopic record favors fossil sources flat in 1980s and 1990s with recent increase, Proceedings of the National Academy of Sciences, 113, 10791–10796, 2016, https://doi.org/10.1073/pnas.1522923113
  - Röckmann, T., Eyer, S., Van Der Veen, C., Popa, M. E., Tuzson, B., Monteil, G., Houweling, S., Harris,

645





- 620 E., Brunner, D., and Fischer, H.: In situ observations of the isotopic composition of methane at the Cabauw tall tower site, Atmospheric Chemistry and Physics, 16, 10469–10487, 2016, https://doi.org/10.5194/acp-16-10469-2016
  - Saboya, E., Zazzeri, G., Graven, H., Manning, A. J., and Englund Michel, S.: Continuous CH<sub>4</sub> and δ<sup>13</sup>CH<sub>4</sub> measurements in London demonstrate under-reported natural gas leakage, Atmospheric Chemistry and Physics, 22, 3595–3613, 2022, https://doi.org/10.5194/acp-22-3595-2022
  - Saunois, M., Martinez, A., Poulter, B., Zhang, Z., Raymond, P. A., Regnier, P., Canadell, J. G., Jackson, R. B., Patra, P. K., and Bousquet, P.: Global methane budget 2000–2020, Earth System Science Data, 17, 1873–1958, 2025, https://doi.org/10.5194/essd-17-1873-2025
- Saunois, M., Stavert, A. R., Poulter, B., Bousquet, P., Canadell, J. G., Jackson, R. B., Raymond, P. A.,
  Dlugokencky, E. J., Houweling, S., and Patra, P. K.: The global methane budget 2000–2017, Earth
  System Science Data, 12, 1561–1623, 2020, <a href="https://doi.org/10.5194/essd-12-1561-2020">https://doi.org/10.5194/essd-12-1561-2020</a>
  - Schaefer, H., Whiticar, M. J., Brook, E. J., Petrenko, V. V., Ferretti, D. F., and Severinghaus, J. P.: Ice record of δ<sup>13</sup>C for atmospheric CH<sub>4</sub> across the Younger Dryas–Preboreal transition, Science, 313, 1109–1112, 2006, https://doi.org/10.1126/science.1126562
- 635 Schaefer, H., Fletcher, S. E. M., Veidi, C., Lassey, K. R., Brailsford, G. W., Bromley, T. M., Dlugokencky, E. J., Michel, S. E., Miller, J. B., and Levin, I.: A 21st-century shift from fossil-fuel to biogenic methane emissions indicated by 13CH4, Science, 352, 80–84, 2016, <a href="https://doi.org/10.1126/science.aad2705">https://doi.org/10.1126/science.aad2705</a>
- Shindell, D., Kuylenstierna, J. C., Vignati, E., van Dingenen, R., Amann, M., Klimont, Z., Anenberg, S. C., Muller, N., Janssens-Maenhout, G., and Raes, F.: Simultaneously mitigating near-term climate change and improving human health and food security, Science, 335, 183–189, 2012, <a href="https://doi.org/10.1126/science.1210026">https://doi.org/10.1126/science.1210026</a>
  - Tans, P. P., Crotwell, A. M., and Thoning, K. W.: Abundances of isotopologues and calibration of CO<sub>2</sub> greenhouse gas measurements, Atmospheric Measurement Techniques, 10, 2669–2685, 2017, https://doi.org/10.5194/amt-10-2669-2017
  - Tuzson, B., Mohn, J., Zeeman, M. J., Werner, R. A., Eugster, W., Zahniser, M. S., Nelson, D. D., McManus, J. B., and Emmenegger, L.: High precision and continuous field measurements of  $\delta^{13}$ C and  $\delta^{18}$ O in carbon dioxide with a cryogen-free QCLAS, Applied Physics B, 92, 451–458, 2008, https://doi.org/10.1007/s00340-008-3085-4
- Van Dingenen, R., Crippa, M., Maenhout, G., Guizzardi, D., and Dentener, F.: Global trends of methane emissions and their impacts on ozone concentrations, JRC Science for Policy Report, 2018, ISBN 978-92-79-96550-0, doi:10.2760/820175, JRC113210
  - Wahl, E. H., Fidric, B., Rella, C. W., Koulikov, S., Kharlamov, B., Tan, S., Kachanov, A. A., Richman, B. A., Crosson, E. R., and Paldus, B. A.: Applications of cavity ring-down spectroscopy to high precision isotope ratio measurement of <sup>13</sup>C/<sup>12</sup>C in carbon dioxide, Isotopes in Environmental and Health Studies, 42, 21–35, 2006, <a href="http://dx.doi.org/10.1080/10256010500502934">http://dx.doi.org/10.1080/10256010500502934</a>
  - Welp, L. R., Keeling, R. F., Weiss, R. F., Paplawsky, W., and Heckman, S.: Design and performance of a Nafion dryer for continuous operation at CO<sub>2</sub> and CH<sub>4</sub> air monitoring sites, Atmospheric Measurement Techniques, 6, 1217–1226, 2013, <a href="https://doi.org/10.5194/amt-6-1217-2013">https://doi.org/10.5194/amt-6-1217-2013</a>
- Wen, X.-F., Meng, Y., Zhang, X.-Y., Sun, X.-M., and Lee, X.: Evaluating calibration strategies for isotope ratio infrared spectroscopy for atmospheric <sup>13</sup>CO<sub>2</sub>/<sup>12</sup>CO<sub>2</sub> measurement, Atmospheric Measurement Techniques, 6, 1491–1501, 2013, <a href="https://doi.org/10.5194/amt-6-1491-2013">https://doi.org/10.5194/amt-6-1491-2013</a>
  - Werner, R. A. and Brand, W. A.: Referencing strategies and techniques in stable isotope ratio analysis, Rapid Communications in Mass Spectrometry, 15, 501–519, 2001, https://doi.org/10.1002/rcm.258